AGU PUBLICATIONS

JGR

Journal of Geophysical Research: Oceans

RESEARCH ARTICLE

10.1002/2014JC009858

Key Points:
- Small differences in forcing lead to differences in OMZ features
- The secondary Tsuchiya jet plays a key role in simulating a most realistic OMZ

Correspondence to:
I. Montes,
imontes@igp.gob.pe

Citation:
Montes, I., B. Dewitte, E. Gutknecht, A. Paulmier, I. Dadou, A. Oschlies, and V. Garçon (2014), High-resolution modeling of the Eastern Tropical Pacific oxygen minimum zone: Sensitivity to the tropical oceanic circulation, *J. Geophys. Res. Oceans*, *119*, 5515–5532, doi:10.1002/2014JC009858.

Received 30 JAN 2014
Accepted 1 JUL 2014
Accepted article online 8 JUL 2014
Published online 27 AUG 2014

High-resolution modeling of the Eastern Tropical Pacific oxygen minimum zone: Sensitivity to the tropical oceanic circulation

Ivonne Montes[1,2,3], Boris Dewitte[1], Elodie Gutknecht[1], Aurélien Paulmier[1,4], Isabelle Dadou[1], Andreas Oschlies[2], and Véronique Garçon[1]

[1]Laboratoire d'Etudes en Géophysique et Océanographie Spatiales, CNRS/CNES/UPS/IRD, UMR 5566, Toulouse, France, [2]GEOMAR Helmholtz Centre for Ocean Research, Kiel, Germany, [3]Instituto Geofísico del Perú (IGP), Lima, Peru, [4]Instituto del Mar del Perú (IMARPE), Callao, Peru

Abstract The connection between the equatorial mean circulation and the oxygen minimum zone (OMZ) in the Eastern Tropical Pacific is investigated through sensitivity experiments with a high-resolution coupled physical-biogeochemical model. A validation against in situ observations indicates a realistic simulation of the vertical and horizontal oxygen distribution by the model. Two sets of climatological open-boundary conditions for the physical variables, which differ slightly with respect to the intensity and vertical structure of the Equatorial Current System, are shown to lead to contrasting characteristics of the simulated OMZ dynamics. From a Lagrangian perspective, the mean differences near the coast originate to a large extent from the different transport of deoxygenated waters by the secondary Tsuchiya Jet (secondary Southern Subsurface Countercurrent, sSSCC). The O_2 budget further indicates a large difference in the balance between tendency terms, with advection exhibiting the largest difference between both simulations, which is shown to result from both linear and nonlinear advection. At regional scale, we also find that the variability of the physical contribution to the rate of O_2 change is one order of magnitude larger than the variability associated with the biogeochemical contribution, which originates from internal high-frequency variability. Overall our study illustrates the large sensitivity of the OMZ dynamics to the equatorial circulation.

1. Introduction

The Eastern Tropical Pacific hosts one of the four eastern boundary upwelling systems named the Humboldt Current System, which is generally viewed to be the most productive of the world oceans, with the northern Humboldt Current System off Peru alone producing about 10% of the world fish catch [*Chavez et al*., 2008].

The Peru Current System localized in the northern part of the Humboldt Current System encompasses one of the most extended oxygen minimum zones (OMZ) [*Fuenzalida et al*., 2009; *Paulmier and Ruiz-Pino*, 2009]. This OMZ is maintained due to the combination of the sluggish oceanic circulation and the high or moderate productivity in the surface layers leading to elevated organic matter export and decomposition consuming dissolved oxygen [*Wyrtki*, 1962; *Helly and Levin*, 2004; *Fuenzalida et al*., 2009; *Paulmier and Ruiz-Pino*, 2009].

A particular feature of the Peru Current System is, due to its proximity to the equator and the coastline characteristics, the strong influence of the remote variability exerted by the equatorial dynamics at a variety of time scales. Whereas at intraseasonal frequencies, the equatorial Kelvin wave is mostly influencing the coastal upwelling as it is trapped along the coast [*Enfield*, 1987; *Clarke and Ahmed*, 1999; *Dewitte et al*., 2011], at lower frequencies both wave activity and change in mean circulation are participating to change the water properties at regional scales. For instance, the interannual equatorial waves associated with the eastern Pacific El Niño result in a drastic change of the circulation due to the radiation of extratropical Rossby waves [*Vega et al*., 2003; *Ramos et al*., 2008] and the alongshore geostrophic adjustment resulting from the advection of warm waters to the south [*Colas et al*., 2008; *Dewitte et al*., 2012], which is associated with the deepening of the oxycline [*Morales et al*., 1999]. The Equatorial Current System also exhibits significant variability at seasonal to interannual time scales [*Kessler*, 2006], which has an impact on the eastward

transport of water masses into the Peru Current System. Observational and modeling studies show that the main subsurface currents forming part of the Equatorial Current System (Equatorial Undercurrent: EUC, primary and secondary Southern Subsurface Countercurrents: pSSCC and sSSCC—also known as Tsuchiya Jets) find their final destination in the Eastern Tropical Pacific [e.g., *Furue et al*., 2007, and references therein] and contribute substantially to feed the Peru-Chile Undercurrent (PCUC) [e.g., *Montes et al*., 2010]. The PCUC is widely recognized as a main source for the coastal upwelling off Peru and northern Chile [*Huyer et al*., 1987; *Albert et al*., 2010] and as the transport route of water with low oxygen and high nutrient concentrations [*Atkinson et al*., 2004]. On the oxygen supply side, the eastward equatorial subsurface currents originating from a well-oxygenated region are associated with a gradual decrease in O_2 concentration as they flow eastward. Although the oxygen supply is different among the various branches of the eastward flow, they are clearly contributing to carrying waters with high oxygen concentrations to the OMZ [*Stramma et al*., 2010], thus taking part in the ventilation of the OMZ [*Karstensen et al*., 2008]. Roughly, the oxygen-richer waters are transported by the EUC while the oxygen-poorer waters are carried by the sSSCC. Therefore, the water mass properties within the PCUC core result from a delicate balance between different sources in terms of oxygen.

Although both dynamical and biogeochemical factors should be considered for understanding the OMZ formation, maintenance, and ventilation [e.g., *Paulmier et al*., 2006, for the OMZ off Chile], previous studies [e.g., *Lam et al*., 2009; *Hamersley et al*., 2007; *Keeling and Garcia*, 2002; *Kalvelage et al*., 2012] have been mainly focused on studying the marine biogeochemical cycle of nitrogen through its fundamental interactions with oxygen via the processes of aerobic remineralization, denitrification, nitrification, nitrogen fixation, and anammox. This is because it has been found that these biogeochemical processes might directly affect global biogeochemical cycles and the life of marine organisms. Moreover, probably due to scarce spatial and temporal data distribution, very few studies have focused on the spatiotemporal variability of the OMZ associated to the Humboldt Current System dynamics and its connection with equatorial variability. The following aspects illustrate the difficulties to be overcome when addressing the OMZ dynamics in the Humboldt Current System by numerical modeling: (1) parameterizations of the biogeochemical models generally differ among models applied to different regions, so caution is required when transferring one model from one region to another one, (2) in the Peru Current System, a previous ocean modeling study [*Echevin et al*., 2011] revealed a particularly large sensitivity of the main features of the circulation (e.g., PCUC characteristics) to the difficult-to-constrain open-boundary conditions. In addition, most physical process-oriented studies have, so far, used models with a rather coarse resolution [*Gnanadesikan et al*., 2012].

In this study, we investigate the dynamical relationship between equatorial circulation and OMZ and assess the sensitivity of the Eastern Tropical Pacific OMZ characteristics (e.g., thickness and intensity of the OMZ) to the representation of the equatorial circulation in a high-resolution coupled physical-biogeochemical model. The model is set up in a climatological configuration similar to *Montes et al*. [2010] so that the focus is on the mean OMZ dynamics (section 2.1). We first show that our system can well reproduce the main OMZ features in this region (section 2.3), which allows for sensitivity experiments with respect to the ocean boundary conditions (section 3). Then, through a Lagrangian approach, we evaluate the oxygen transport between the Equatorial Current System and PCUC, emphasizing on the main branches connecting both current systems. The experiments allow identifying that the sSSCC is a key feature of the sensitivity of the OMZ to the equatorial circulation. Then, we use an explicit O_2 budget to further investigate the differences in OMZ dynamics due to the different background conditions (both O_2 and mean circulation) between simulations with distinct ocean boundary conditions (section 3.4). It is shown that, despite an overall comparable mean OMZ structure, there is a significantly different balance between physical and biogeochemical processes within the energetic coastal current system between the simulations with different prescribed inflow from the western tropical Pacific, illustrating the large sensitivity of the OMZ dynamics to the open-boundary conditions.

2. Methodology

2.1. High-Resolution Coupled Physical-Biogeochemical Model

In this study, we employed a modeling approach consisting of the hydrodynamic model ROMS (Regional Ocean Model System) [see *Shchepetkin and McWilliams*, 2009, 2005, for a complete description of the

model] coupled with the nitrogen-based *Bio*geochemical model developed for the *E*astern *B*oundary *U*pwelling *S*ystems (BioEBUS) [*Gutknecht et al*., 2013a, 2013b, see Appendix A for a brief model description] that consists of two compartments ("small" and "large") of phytoplankton, zooplankton, and detritus, dissolved organic nitrogen and the nutrients nitrate, nitrite and ammonium, as well as nitrous oxide. It is employed here in two climatological configurations, which were formerly analyzed and validated for the Eastern Tropical Pacific, being called ROccam and RSoda [*Penven et al*., 2005; *Montes et al*., 2010; *Echevin et al*., 2011]. These solutions reproduce realistically the mean to seasonal circulation in the Peru Current System from the regional model setup used in this study. Only a few differences between these configurations exist which, as will be shown below, can still significantly impact the simulated O_2 distribution (more details of the differences in the mean circulation can be found in the Appendix of *Montes et al*. [2010] and in *Echevin et al*. [2011]).

Both configurations cover the region originally used by *Penven et al*. [2005] ranging from 4°N to 20°S and from 70°W to 90°W and having a horizontal resolution of 1/9° (∼12 km) with 32 sigma levels in the vertical (higher resolution in the upper ocean). The bottom topography and coastline are interpolated from the 2′ resolution ETOPO2 database [*Smith and Sandwell*, 1997]. Models are forced by the monthly wind stress climatology computed from QuikSCAT satellite scatterometer data [*Liu et al*., 1998] and by heat and freshwater fluxes derived from the COADS ocean surface monthly climatology [*Da Silva et al*., 1994]. For the three open-boundary conditions, a monthly climatology derived from the Ocean Circulation and Advance Modelling project (OCCAM) global ocean model [*Saunders et al*., 1999] is used to provide the dynamical variables (temperature, salinity, and velocity fields) for ROccam while a monthly climatology computed from the Simple Ocean Data Assimilation (SODA) reanalysis [*Carton and Giese*, 2008] is used for RSoda. The biogeochemical variables, for both configurations, are extracted from the CSIRO Atlas of Regional Seas [CARS, 2009, http://www.cmar.csiro.au/cars; for nitrate and oxygen concentrations] and SeaWiFS [*McClain et al*., 1998; *O'Reilly et al*., 2000; for chlorophyll *a* concentration]. Other biogeochemical tracers are computed following the methodology of *Gutknecht et al*. [2013a, 2013b]. Initial phytoplankton is a function of satellite-derived Chl *a* vertically extrapolated from the surface using *Morel and Berthon* [1989] parameterization. Based on *Koné et al*. [2005], a cross-shore profile following in situ observations is applied for zooplankton, decreasing from onshore to offshore, and a vertical (exponential) constant profile is used for detritus (NO_2, NH_4, and DON). The nitrous oxide (N_2O) is computed as a function of oxygen following *Suntharalingam et al*. [2000, 2012].

The simulations were performed over a 22 year period. The first 13 years were run with the physical model component only the next 9 years were run with the coupled physical-biogeochemical model. Note that "coupled" here only refers to the influence of the oceanic circulation on the biogeochemical processes but not the opposite. The modeled biogeochemistry reached a statistical equilibrium (in terms of surface-averaged and volume-averaged biogeochemical variables, e.g., oxygen and nutrient content) after 4 years; therefore, the last 5 years of simulations (Y18–Y22) were used to analyze the coupled model performance as well as the difference between both simulations. Model outputs were stored as three-daily averages.

2.2. Lagrangian Diagnostics

The changes in oxygen content between the Equatorial Current System and the Peru-Chile Undercurrent (PCUC) are investigated using a Lagrangian approach [*Capet et al*., 2004; *Carr et al*., 2008, ROMS-offline tracking module] that calculates trajectories of numerical floats (particles) from the simulated velocity fields. For both simulations, our Lagrangian experiment consists in launching three groups of floats in the 18th year and integrating these forward in time for 2 years. Each group, composed of 1500 floats, is randomly distributed on a vertical section at 88°W at strategic locations within the equatorial subsurface currents: EUC (bounded from 1°N to 1°S and between 50 and 250 m depth), pSSCC (bounded from 3°S to 5°S and between 50 and 300 m depth), and sSSCC (bounded from 6°S to 8°S and between 50 and 300 m depth). These strategic locations, defined as boxes, are identified from the inspection of vertical sections of annual mean zonal velocities extracted from both simulations at 88°W (Figures 2d and 2e). As these solutions exhibit a slightly different vertical structure of equatorial subsurface currents, boxes are defined to adjust both observed currents. The floats are supposed to be neutrally buoyant and are advected forward in time by the 3 day average velocity field linearly interpolated onto the locations of the individual floats. Recorded along the pathway of each float is its position (longitude, latitude, and depth), oxygen concentration, and oxygen changes provided from both physical and biogeochemical fluxes oxygen source and sink terms. For

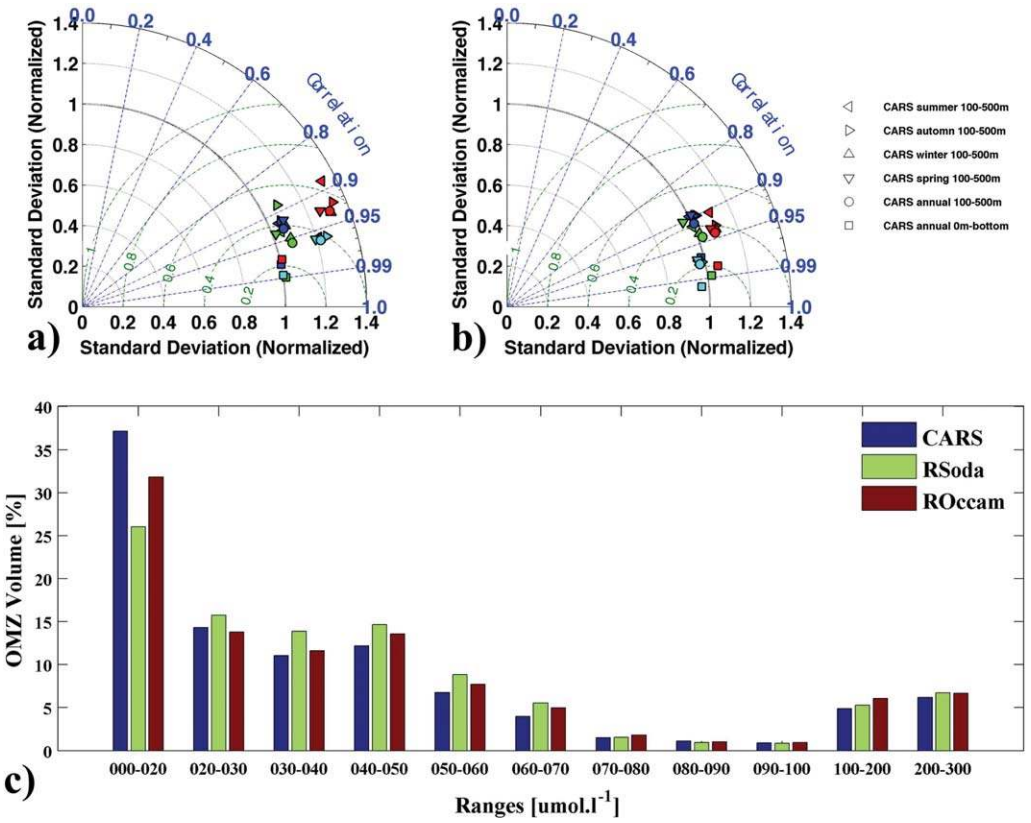

Figure 1. Taylor diagram of the seasonal and annual mean patterns of temperature (light blue), salinity (red), nitrate (green), and oxygen (blue) vertically averaged between 100 and 500 m depth generated from (a) ROccam and (b) RSoda showing the relative skill of our coupled solutions in simulating the spatial pattern of dynamical and biogeochemical variables. Basically, we computed the seasonal and annual mean horizontal maps of temperature, salinity, and nitrate and oxygen concentrations between 100 and 500 m depth (to focus on the OMZ core) for both modeled and observational data (CARS). Additionally, we included the annual mean of each chosen variable calculated over the whole water column. (c) Ocean volume distribution as a function of the oxygen content (μmol l^{-1}) computed above the 1000 m depth from CARS (in blue), ROccam (in red), and RSoda (in green); expressed in percentage of total volume.

our analysis, only floats reaching the ∼9°S cross-section offshore Peru are counted (see section 3.4, for further description of this criterion).

2.3. Model Assessment

Figure 1 provides a statistical evaluation of the RSoda and ROccam model skills, both in terms of physical (e.g., temperature and salinity) and biogeochemical (e.g., nitrate and oxygen) variables, in the form of Taylor's diagrams [*Taylor*, 2001] for both the annual mean and seasonal cycles. Basically, we compute the seasonal and annual mean patterns of temperature, salinity, and nitrate and oxygen concentrations between 100 and 500 m depth (to focus on the OMZ core) for both modeled (ROccam and RSoda) and observational data as derived from CARS. CARS is used as a benchmark for the validation because it has a refined treatment of the data interpolation near steep topography compared to the World Ocean Atlas (WOA). It should be kept in mind that, like WOA, this data set could still have errors in low sampling areas [*Bianchi et al*., 2012]. Grey isolines provide a measure of skill, as defined by equation (4) in *Taylor* [2001]. The radial coordinate gives the magnitude of total standard deviation, normalized by the observed value, and the angular coordinate gives the correlation with observations. It follows that the distance between the observed point and any model's point is proportional to the root-mean-square (RMS) model error. The validation indicates that the model has skill in simulating the main features of the OMZ. For annual mean conditions, all variables analyzed over a domain (100–500 m depth) that encompasses the OMZ reach pattern correlations with data larger than 0.85 both for ROccam and RSoda as well as low standard deviations (i.e., in the order of the observed values). Centered RMS differences are relatively small ($<$0.5 of the field's variance) in both cases, with RSoda having the smallest values and spread among parameters. A comparable skill is found for the seasonal cycle and the annual mean over the whole water column.

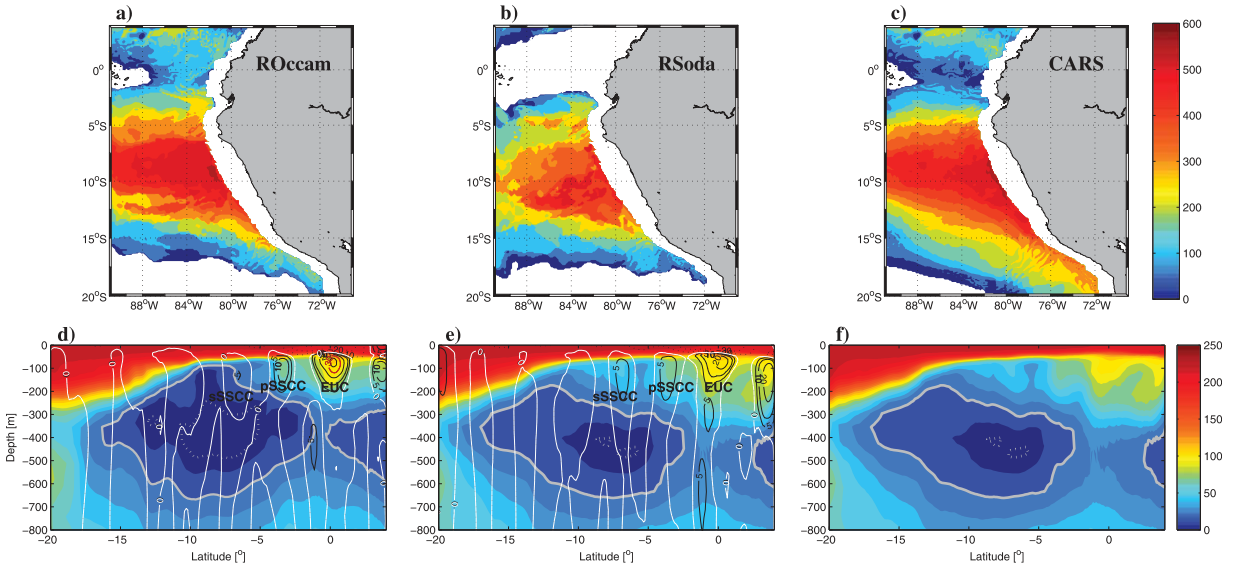

Figure 2. (top) The annual mean OMZ thickness (O_2 <20 μmol l^{-1}) for (a) ROccam, (b) RSoda, and (c) CARS. (bottom) Vertical sections of annual mean oxygen at 88°W extracted from (d) ROccam, (e) RSoda, and (f) CARS, oxygen concentration of 20 μmol l^{-1} is depicted as a white thick contour. Eastward zonal velocities are contoured with black lines (contour interval every 5 cm s^{-1}—thick black (red) contour corresponds to 5 cm s^{-1} (30 cm s^{-1})) and marked with their respective magnitude in ROccam and RSoda.

The results of Figure 1 also indicate that both simulations are almost indistinguishable in terms of their skill in simulating the main features of the region. RSoda is apparently more realistic in terms of salinity and temperature, in agreement with *Echevin et al*. [2011]. Discrepancies can be also observed between RSoda and ROccam in terms of oxygen, with ROccam providing better model-data pattern correlations than RSoda, and RSoda yielding standard deviations not as good as those obtained with ROccam.

In the following, we investigate the reasons for these differences between both model solutions.

3. Results and Discussion

3.1. Oxygen Content in the Eastern Tropical Pacific

To gain further insight into the differences in OMZ characteristics of the two simulations, we analyze the volume distribution of O_2 concentrations over the whole water column (Figure 1c). For both solutions, the distributions (used here as a metric for quantifying differences between simulations) are computed over the domain (70°W–90°W/4°N–20°S) and for different oxygen concentration bins between 0 and 300 μmol l^{-1}.

Both model solutions show a comparable distribution of oxygen concentrations, which agrees reasonably well with the distribution obtained from data (Figure 1c). According to the CARS database, the well-oxygenated layers (>100 μmol l^{-1}) occupy ∼12% of the total volume in the upper 1000 m of the water column, layers where oxygen varies between 70 and 100 μmol l^{-1} occupy only ∼4%, layers between 20 and 70 μmol l^{-1} ∼48% and low-oxygen waters (<20 μmol l^{-1}, range defined by *Kamykowsi and Zentara* [1990] as the OMZ, see also *Paulmier and Ruiz-Pino* [2009]) occupy ∼36%. Both model solutions are in good agreement with this oxygen data distribution except in the layers with concentrations below 70 μmol l^{-1}. In ROccam and RSoda, layers between 20 and 70 μmol l^{-1} (hereafter referred to as intermediate waters) occupy ∼52% and ∼60%, respectively, while the modeled OMZ (layer <20 μmol l^{-1}) accounts for about 32% of the total volume in ROccam and only ∼26% in RSoda. Thus, the OMZ volume in ROccam is close to the one derived from observations whereas it is underestimated in RSoda. Such a reduction in the OMZ core in RSoda represents a decrease of ∼28% of the core region as compared to observations and ∼19% as compared to ROccam. Moreover, the larger extent of the intermediate oxygen levels in RSoda corresponds to an increase of ∼25% as compared to observations and ∼13% as compared to ROccam. Therefore, the oxygen classes most impacted by the open-boundary conditions are those corresponding to oxygen concentrations below 70 μmol l^{-1}, specifically those located in the OMZ (<20 μmol l^{-1}). Such differences in OMZ characteristics between both simulations are related to the differences in the vertical structure of the

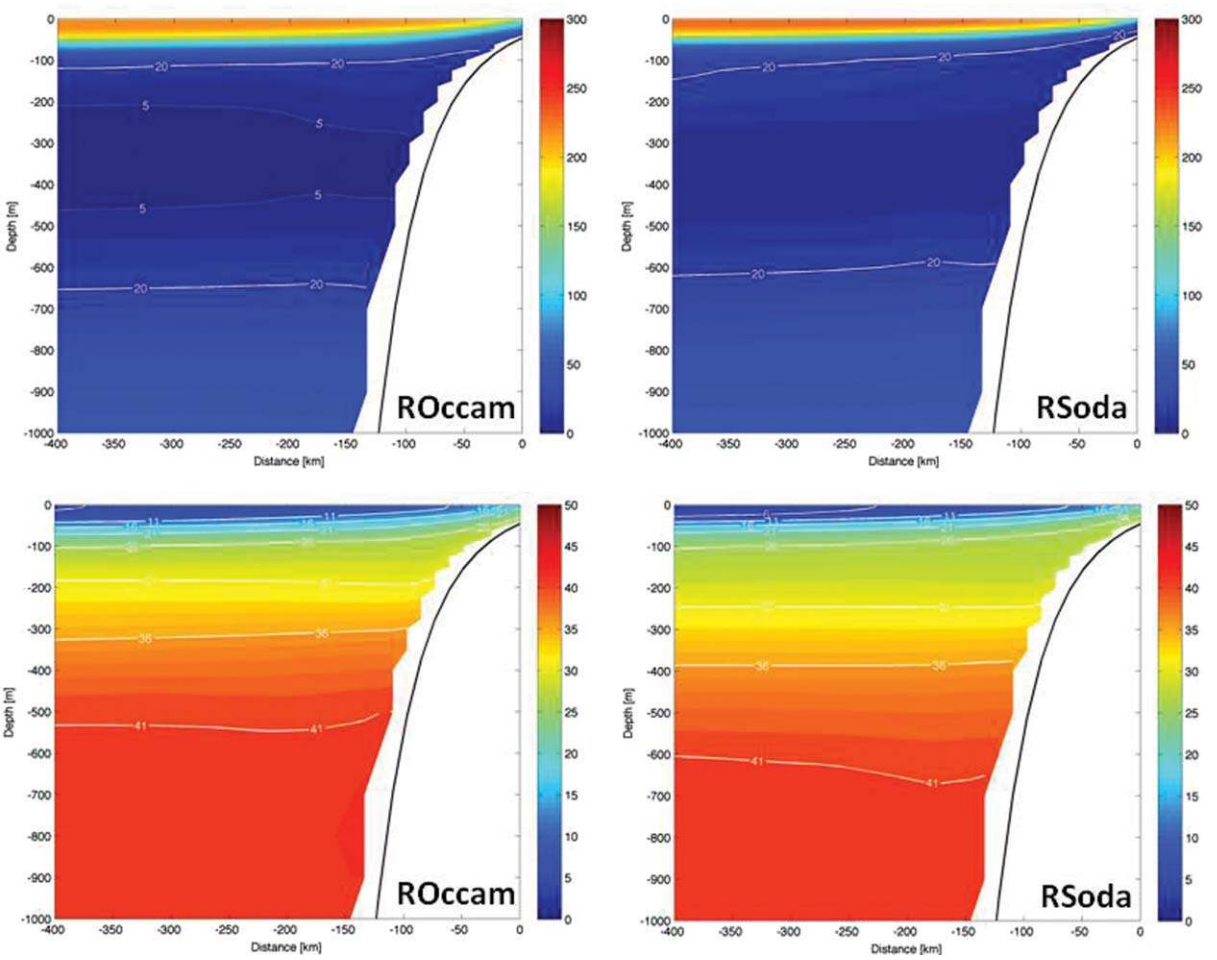

Figure 3. (top) Vertical sections of annual mean oxygen (in μmol l^{-1}) and (bottom) nitrate (NO_3) concentrations (in μmol l^{-1}) averaged between 7°S and 13°S extracted from (left) ROccam and (right) RSoda. Oxygen concentration of 20 μmol l^{-1} is depicted as white contour lines and 5 μmol l^{-1} as white dotted lines.

equatorial subsurface currents that modify the balance between biogeochemical and physical contributions to the O_2 budget within the OMZ as shown in section 3.3.

3.2. Vertical and Horizontal Extent of the Eastern Tropical Pacific OMZ

Since the largest differences between the simulations are found in the OMZ core (O_2 classes <20 μmol l^{-1}), we now focus on the OMZ thickness which serves here as a metric for diagnosing the differences between ROccam and RSoda (Figures 2a–2c). In ROccam, a maximum vertical thickness of 550 m develops close to the coast of Peru. The OMZ presents a tongue-like shape extending offshore. Its northern limit is zonally oriented while its southern boundary presents a pronounced northwest-southeast orientation between 15°S and 19°S. In contrast, the OMZ simulated in RSoda is confined to a region close to the coast of Peru and only extends offshore between 9°S and 12°S, reaching a maximum vertical thickness of 500 m. North and south of this core, the limits of the OMZ are located near 2°S and 18°S, respectively. The spatial correlation between simulations and observations (within the latitudinal range 5°S–15°S) confirms that ROccam is more skillful in representing the OMZ thickness (c = 0.88 (0.69) for ROccam (RSoda)).

Although the maximum thickness in both solutions is comparable, the vertical and horizontal extensions of the OMZ exhibit large differences, which can be interpreted in terms of the differences in the vertical distribution of NO_3 because the supply of nutrients impacts the oxygen demand. In particular, RSoda presents an underestimation of NO_3 concentrations as compared to ROccam (Figure 3). Reduced nutrient concentrations yield a lower productivity and therefore a diminished oxygen demand. The differences in vertical and

Table 1. Estimation of O_2 Fluxes in ROccam and RSoda Simulations[a]

	EUC [2N–2S/0–450 m]			pSSCC [2–6S/0–450 m]			sSSCC [6–9S/0–450 m]		
Coupled Solutions (Roms-BioEBUS)	O_2 Flux (10^3mol s^{-1})	Maximum Velocity (cm s^{-1})	Transport (Sv)	O_2 Flux (10^3 mol s^{-1})	Maximum Velocity (cm s^{-1})	Transport (Sv)	O_2 Flux (10^3 mol s^{-1})	Maximum Velocity (cm s^{-1})	Transport (Sv)
ROccam-BioEBUS	366.1	40	7.75	76.6	15	2.76	9.2	5	0.81
RSoda-BioEBUS	244.1	25	5.2	71	7	2.44	42.2	7	1.82
O_2 flux in the PCUC (∼9°S) originated from:			EUC			pSSCC			sSSCC
ROccam-BioEBUS			18			23			5
RSoda-BioEBUS			12			21			23

[a](top) Eastward oxygen fluxes (in 10^3 mol s^{-1}), maximum mean velocities (cm s^{-1}), and transports (Sv) associated with each equatorial subsurface current at 88°W obtained from Eulerian experiment by ROccam and RSoda. (bottom) Estimation of oxygen that corresponds to water parcels originating from each equatorial subsurface current at 88°W reaching the PCUC core at ∼9°S. The reader is referred to *Montes et al.* [2010] for details on this calculation.

horizontal structures may also originate from differences in the simulated Equatorial Current System that lead to differences in the transport of oxygen and nutrients into the OMZ, as we shall see below.

3.3. The Equatorial Current System and the Oxygen Content

In this section, we provide evidence that differences in the OMZ characteristics described earlier between ROccam and RSoda are related to their differences in simulating the Equatorial Current System. A Lagrangian description developed by *Montes et al.* [2010] for the Eastern Tropical Pacific traces the sources and pathways of the PCUC waters. They find that the feeding sources of the PCUC are mainly the subsurface currents forming part of the Equatorial Current System (EUC, pSSCC, and sSSCC). Hence, the focus here is on these three main components of the ECS.

Despite an overall good agreement between both simulations, the Eulerian diagnostics reveal notable differences in the vertical extension and intensity of the three main PCUC sources (Figures 2d, 2e, and Table 1). The EUC is located between 1.5°N and 1.5°S, it extends from 30 to 200 m depth and is accompanied by a high oxygen concentration in both simulations (Figures 2d and 2e), which is consistent with previous studies [e.g., *Lukas et al.*, 1986; *Stramma et al.*, 2010; *Echevin et al.*, 2011]. The EUC is the key player in ventilating the OMZ by carrying oxygen-rich waters along the equator. This eastward subsurface flow reaches a maximum mean velocity of 25 cm s^{-1} in RSoda while it is stronger (40 cm s^{-1}) in ROccam (Figures 2d and 2e). The pSSCC is located between 3°S and 4.5°S and extends from about 40 to 200 m depth in both solutions. However, their subsurface cores flow eastward with a different maximum mean velocity of about 15 cm s^{-1} (ROccam) and 7 cm s^{-1} (RSoda). Its associated oxygen concentration at 88°W is about half of that exhibited by the EUC. The sSSCC (between 6°S and 8°S), which is situated south of the pSSCC, has a wider vertical extent in ROccam than in RSoda. It flows with a maximum velocity of 7 cm s^{-1} in RSoda and slightly less (∼5 cm s^{-1}) in ROccam. In both model solutions, the sSSCC oxygen concentration is at least half of that of the pSSCC. While weaker in strength than the pSSCC, the sSSCC carries relatively oxygen-poor waters into the PCUC in agreement with *Karstensen et al.* [2008] and *Stramma et al.* [2010].

The latitudinal differences in the oxygen signal of each eastward equatorial subsurface current and associated supply of oxygen-rich waters to the OMZ were previously documented by *Stramma et al.* [2010] from hydrographic data (meridional cross-equatorial sections along 170°W, 140°W, 125°W, 95°W, and ∼85°W). Here the modeled oxygen fluxes and mass transports cannot strictly be compared with *Stramma et al.*'s [2010] results due to differences in methodology (in particular they followed a density criterion and employed different density surfaces for their estimations). However, the model solutions exhibit comparable features as the observations. At 88°W, the largest oxygen fluxes available to ventilate the OMZ are associated with the EUC and pSSCC in both solutions. These fluxes are significantly stronger in ROccam than in RSoda (+50% for the EUC in ROccam as compared to RSoda), mostly due to stronger currents simulated in ROccam (Table 1). The higher fluxes in ROccam could partially explain the differences in the OMZ thickness (Figures 2a and 2b) since, this could trigger aerobic processes (e.g., oxic decomposition and nitrification) that enhance the oxygen utilization and nutrient availability through organic matter degradation, leaving, as a consequence, the water column depleted of oxygen (see section 3.4). On the other hand, the sSSCC

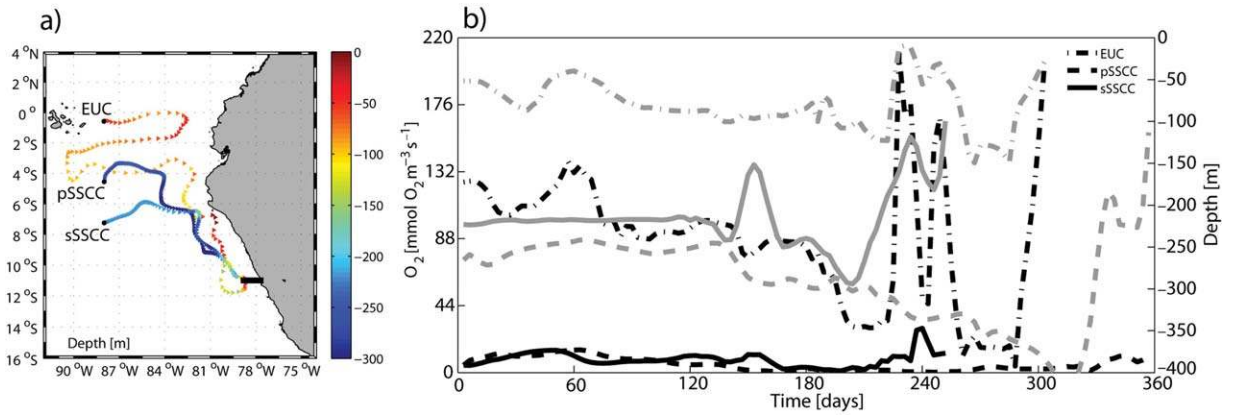

Figure 4. (a) Spaghetti diagrams of selected particles showing typical routes of floats associated to each main eastward equatorial subsurface current (EUC, pSSCC, and sSSCC) feeding the PCUC. Black circles are initial positions of each float, colors represent the along-trajectory depth (in m) and, the cross-shore black bar, at ∼9°S, is the PCUC section reaching the floats. Evolution of Figure 4b, the oxygen content (black lines, scale on left axis) and depth (gray lines, scale on right axis) along the float pathways. In Figure 4b, the dash-dotted, dashed, and solid lines indicate the EUC, pSSCC, and sSSCC, respectively.

exhibits an opposite pattern: RSoda simulates an oxygen flux at 88°W almost 5 times larger than in ROccam. This difference is related to the current intensity and associated transport (Table 1) but also to the oxygen content modeled in each solution (Figure 2). The oxygen content is higher in RSoda. This discrepancy between both solutions on the role the sSSCC plays in feeding the OMZ can partially explain the differences in the OMZ thickness (Figures 2a and 2b). Local biogeochemical processes and mesoscale activity could also contribute to such discrepancy [*Brandt et al*., 2010; *Czeschel et al*., 2011].

A Lagrangian analysis applied to both solutions showed that only a small fraction (5%) of the EUC continues flowing eastward from the equatorial region (between 86°W and 87°W) and reaches the coast, while the rest recirculates and contributes to westward flows such as the South Equatorial Current in both simulations. The difference in oxygen distribution in the simulations thus cannot be assigned only to the difference in EUC characteristics. In the case of the Tsuchiya Jets, ∼30% and ∼55% of their total flow (i.e., water carried by the current) is available to form part of the PCUC from the pSSCC and sSSCC, respectively [see *Montes et al*., 2010, for details]. Based on these percentages, an estimate of the oxygen fluxes associated with the EUC and pSSCC indicates that the differences are small between the simulations (18×10^3 mol s^{-1}—ROccam, 12×10^3 mol s^{-1}—RSoda for the EUC, 23×10^3 mol s^{-1}—ROccam, 21×10^3 mol s^{-1}—RSoda for the pSSCC, Table 1). On the other hand, significant differences in the O_2 fluxes are found for the sSSCC (5×10^3 mol s^{-1}—ROccam, 23×10^3 mol s^{-1}—RSoda, Table 1). Such a difference is likely to explain the difference in oxygen distribution between both simulations. *Monteiro et al*. [2006, 2011] suggested that the development of anoxic conditions initially needs a remote equatorial hypoxic (and high-nutrient) condition for triggering the anoxic event after which it can be sustained by a locally active remineralization resulting from local biological export production. Without a remote trigger, the local forcing could not develop anoxic conditions because the physical supply of oxygen would be too high. In our study, the higher oxygen flux provided by the sSSCC in the RSoda simulation implies a larger ventilation of the OMZ and, as a consequence, a more oxygenated water column, consistent with Figure 2e. The latter would be also in agreement with *Brandt et al*.'s [2010] results. They found, by means of a conceptual model developed for the Tropical North Atlantic and observations, that a reduction of the mean OMZ oxygen levels could be attributed to a weakening in the strength of the zonal jets, while they also pointed out that a similar behavior can be achieved by a reduction of the meridional and vertical eddy activity. According to *Echevin et al*. [2011], who use the same open-boundary conditions than in our study, the most significant change resulting from employing different boundary conditions was the mesoscale activity developed in each model (resulting from the different PCUC structures that imply a distinct level of baroclinic instability), which was higher in RSoda than in ROccam. We therefore hypothesize that the more intense mesoscale activity in combination with the higher background oxygen concentration in RSoda yields a more oxygenated water column and, therefore, a smaller OMZ volume. In the next section, we provide an estimate of the O_2 budget to test this hypothesis.

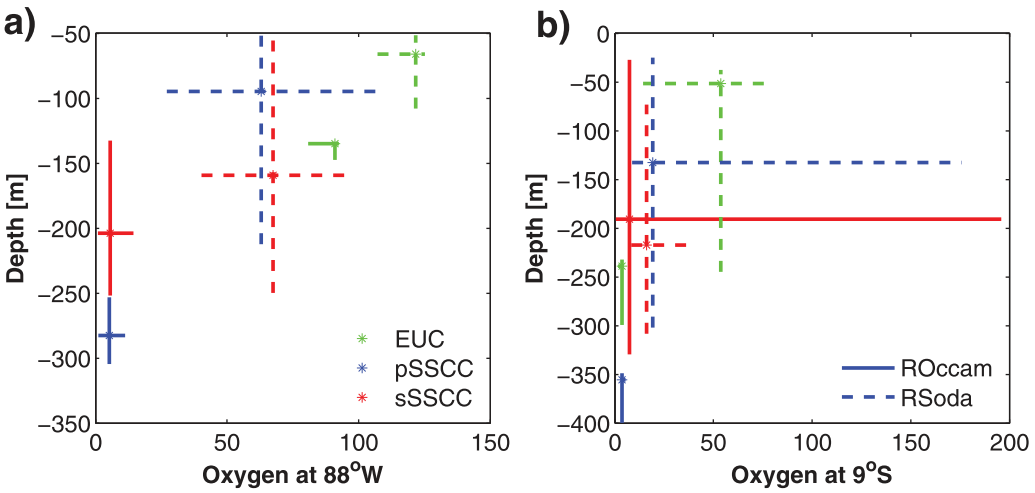

Figure 5. Oxygen distribution for each equatorial source (EUC, pSSCC, sSSCC) at (left) 88°W and (right) 9°S: (a and b) Median oxygen and median depth of the currents together with minimum and maximum values plotted as vertical (depth) and horizontal (concentration) bars for ROccam (solid lines) and RSoda (dashed lines). The statistics were calculated over the period Y18–Y20.

3.4. Tracing Routes and Processes to the PCUC

In order to further document, the fate of waters transported by the ECS into the PCUC, an O_2 budget along the Lagrangian floats trajectories is performed (Figures 4 and 5). The O_2 budget (calculated on-line) provides the contributions of all terms of the O_2 tendency equation (advection, mixing, consumption, production, etc.) at each grid point and time step. The so-called Lagrangian experiment here consisted in releasing numerical floats in each equatorial subsurface current (EUC, pSSCC, and sSSCC) at 88°W (see section 2.2, for details), retaining only the floats whose trajectory reached the cross-shore section at 9°S extending from the coast of Peru to 79°W, i.e., encompassing almost exclusively the PCUC. All the tendency terms are recorded along the retained float trajectories. This experiment is guided by the consideration that about 30% of the PCUC is fed by the three main eastward subsurface equatorial currents, i.e., EUC, pSSCC, and sSSCC [see *Montes et al.*, 2010, for details]. Such an approach allows tracing back the modeled oxygen changes and the contributions of both physical and biogeochemical fluxes (i.e., tendency terms) along the main paths of the Equatorial Current System to the PCUC.

The visualization of the generic pathways of a few particles is shown in Figure 4a, along with their associated depth and oxygen concentration that characterize each current from the equatorial region, at 88°W (Figure 4b). The highest oxygen concentrations are associated with the EUC while the lowest are found in the Tsuchiya Jets, especially in the sSSCC, which is in agreement with *Stramma et al.* [2010]. Moreover, the closer inspection of float trajectories indicates that initially, they move eastward in the subsurface (layer between 40 and 400 m depth) with relatively high oxygen content and then, the O_2 content slightly diminishes as they move along their paths (Figures 4a and 4b), flowing zonally toward the coast then to the south. In the particular case of the EUC, the floats flow from 88°W with an average concentration of 120 mmol O_2 m^{-3} along the equator up to ~82°W then, turn southwestward until joining the pSSCC where its oxygen values fall to ~80 mmol O_2 m^{-3}. This overall deoxygenation along the float trajectories is consistent with previous observational studies that report the presence of the longitudinal oxygen gradient in the Eastern Tropical Pacific, with oxygen content decreasing eastward [e.g., *Fuenzalida et al.*, 2009; *Stramma et al.*, 2010]. Nevertheless, such deoxygenation along the pathways is interrupted by a sudden increase in oxygen content at an average time of 196 days (with a standard deviation of 79 days). This is mainly controlled by positive horizontal and vertical advection associated with mesoscale activity (not shown) that allows the floats to reach shallower regions and so increase O_2 concentrations mostly via photosynthesis (Figure 4b).

Further analysis of the Lagrangian experiments shows that the floats are associated with low oxygen concentrations in the PCUC regardless of their source regions (Figure 5), unless individual floats are influenced by local processes (i.e., coastal upwelling or local mesoscale activity). In particular, the water masses originating from the EUC and pSSCC are those that experience the largest transformation in terms of O_2 content,

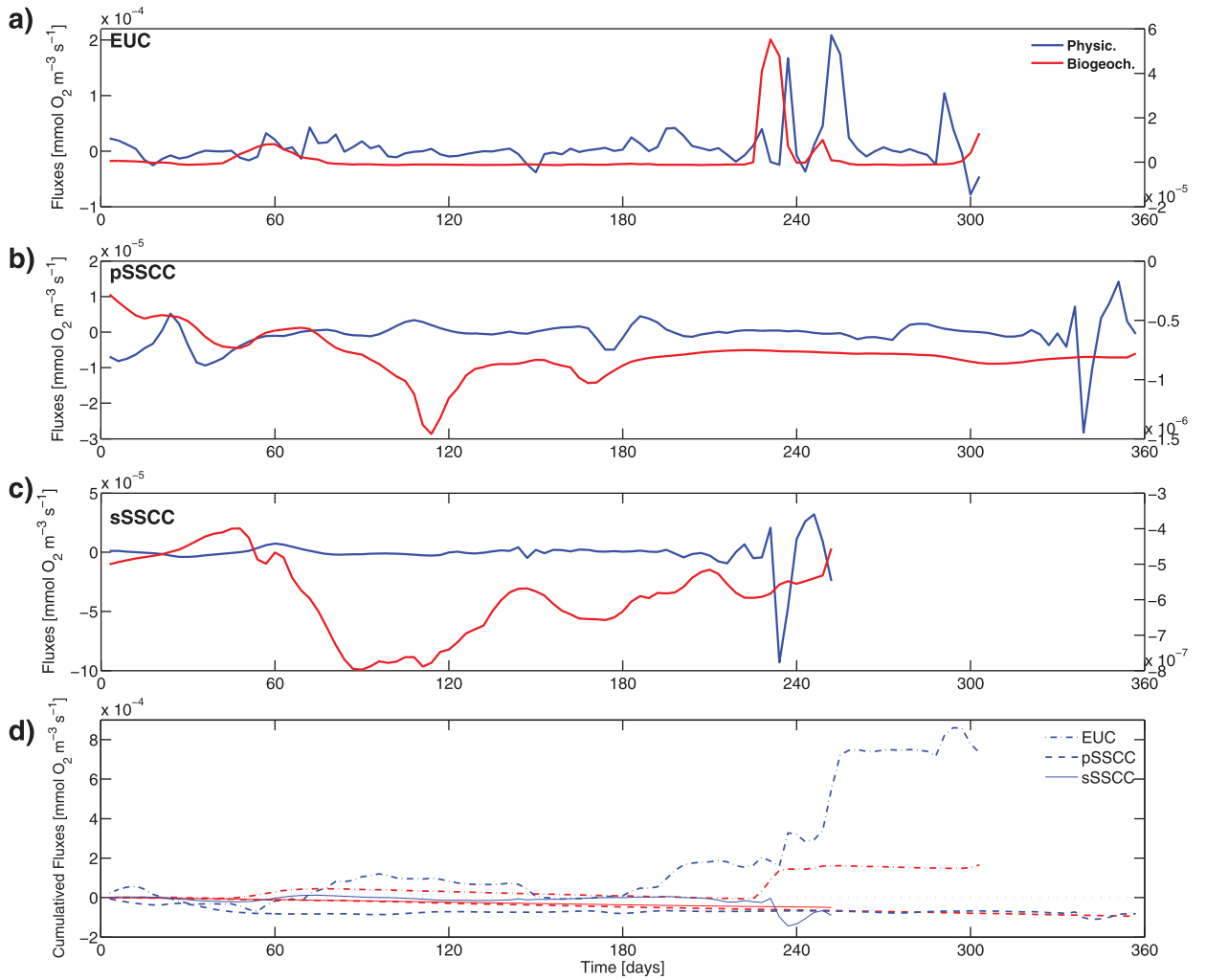

Figure 6. O_2 budget along the main paths of the ECS: evolution of the relative contribution of the physical (blue lines) and biogeochemical (red lines) processes to the O_2 changes along the float pathways of the (a) EUC, (b) the pSSCC, and (c) the sSSCC. The left (right) scale is for the physical (biogeochemical) process. Evolution of Figure 6d, the cumulative contribution of the physical (blue lines) and biogeochemical (red lines) processes to the rate of O_2 change along the paths. In Figure 6d, the dash-dotted, dashed, and solid lines indicate the EUC, pSSCC, and sSSCC, respectively. This scheme is representative for both ROccam and RSoda solutions.

since most floats have a concentration below 20 mmol O_2 m^{-3} when they arrive at 9°S (Figure 5b). Such transformation is allowed by the relatively long time they take to reach the PCUC core (the time for a float released at 88°W to reach the section at 9°S ranges between 4 and 24 months). Floats exhibiting a concentration >20 mmol O_2 m^{-3} at the 9°S section are located in the upper part of the PCUC, i.e., within the upper part of the mean oxycline (see Figure 4b); taking less time to reach the nearshore section. On the other hand, those which reach the oxycline core near the coast experience a drastic change in O_2 concentration (cf. days 220–260 for EUC and sSSCC floats) that is associated to a complex balance between physical processes and biogeochemical processes (see Figure 6).

Figure 6 presents the relative contribution of the physical and biogeochemical processes to the oxygen changes along the float pathways of the equatorial subsurface currents: EUC, pSSCC, and the sSSCC. In absolute value, physical processes (blue lines) displayed by all currents tend to have larger variations than biogeochemical processes (red lines) but fluctuate around the zero line implying a comparable magnitude in terms of cumulative fluxes (Figure 6d). These accumulative fluxes indicate that the sSSCC and pSSCC tend to deoxygenate the PCUC (since the sum of physical and biogeochemical fluxes is negative, i.e., O_2 consumption), whereas the EUC contributes to increase the O_2 content within the PCUC ($\frac{\partial O_2}{\partial t} > 0$, i.e., net O_2 production at the relatively shallow depth levels of the trajectory). Figure 6 thus indicates that, although

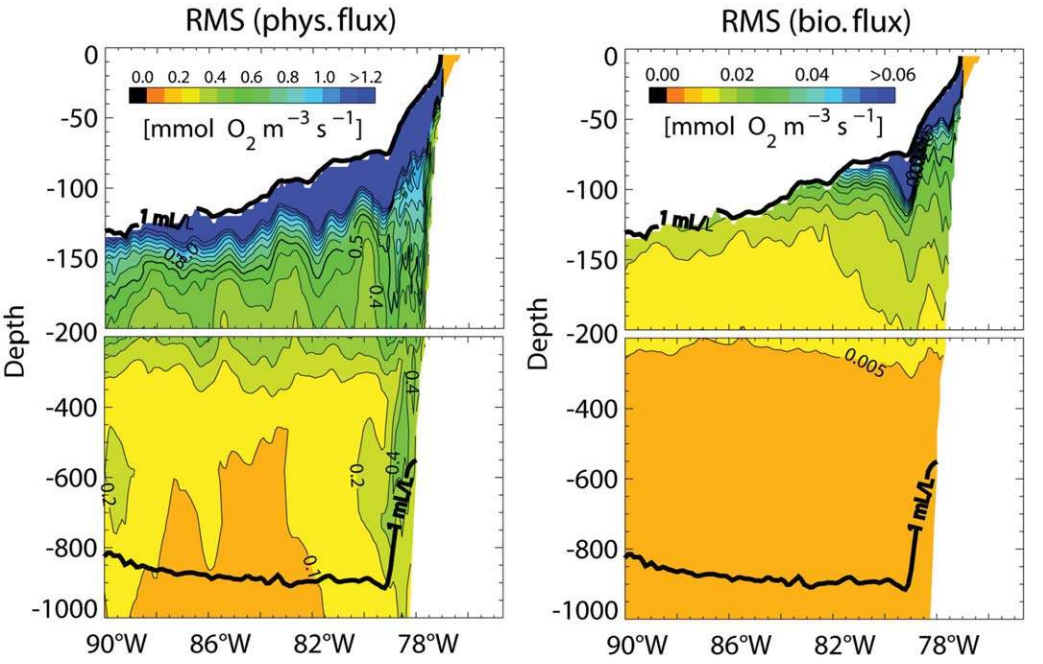

Figure 7. Root mean square of physical and biogeochemical fluxes anomalies (relative to the mean over the whole period) for RSODA at 12°S. The variability is calculated over the period Y18 July–Y20 June.

biogeochemical and physical fluxes on average tend to compensate each other, the different branches of the Equatorial Current System tend to behave as sinks (pSSCC, sSSCC) and sources (EUC) of O_2 content to the PCUC from a Lagrangian view. Figure 6 also reveals that, in general, variations in physical processes are also one order of magnitude larger than variations in biogeochemical processes along the trajectories. For

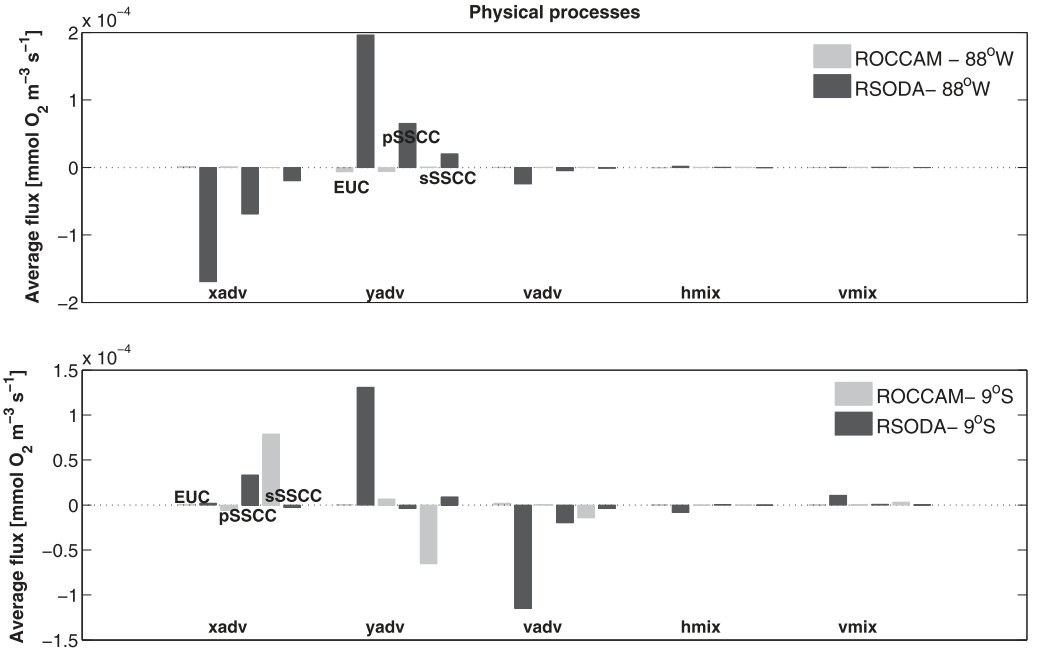

Figure 8. Mean flux of all O_2 terms involved in the physical processes of each equatorial subsurface current computed for both simulations, ROccam (black bars) and RSoda (gray bars), at (top) 88°W and (bottom) 9°S. Physical terms are referred to advection (zonal—xadv, meridional—yadv, vertical—vadv) and mixing (horizontal—hmix, vertical—vmix). Fluxes with negative values represent a sink of oxygen and positive a source. For each process, the first two bars refer to the EUC, the middle bars to the pSSCC, and the last to bars to the sSSCC.

Table 2. Percentage Contributions of All Oxygen Terms Computed From Lagrangian Experiment by RSoda And ROccam[a]

Physical Processes (%)

88°W	xadv	Yadv	vadv	hmix	vmix	Total
EUC—ROccam	15.7	−71.0	4.1	−8.4	−0.9	100
EUC—Rsoda	−43.2	50.1	−6.2	0.5	0.1	100
pSSCC—ROccam	14.0	−78.8	4.9	1.6	0.8	100
pSSCC—Rsoda	−49.4	46.7	−3.5	0.1	0.2	100
sSSCC—ROccam	−9.1	77.1	11.2	2.2	−0.4	100
sSSCC—RSoda	−47.2	48.2	−3.4	−1.0	−0.2	100
9°S						
EUC—ROccam	20.7	12.9	63.2	2.0	1.1	100
EUC—Rsoda	0.8	49.0	−43.1	−3.1	4.0	100
pSSCC—ROccam	−44.6	52.8	2.5	−0.1	0.0	100
pSSCC—Rsoda	57.5	−6.7	−34.0	0.6	1.3	100
sSSCC—ROccam	48.9	−40.4	−8.9	0.0	1.9	100
sSSCC—Rsoda	−17.2	56.6	−25.4	−0.8	0.1	100

Biogeochemical Processes (%)

88°W	Photosynthetic Production	Oxic Decomposition	Excretion	Nitrification	Total
EUC—ROccam	0.5	−76.7	−7.2	−15.6	100
EUC—Rsoda	42.8	−44.6	−4.3	−8.3	100
pSSCC—ROccam	0.0	−72.4	−12.1	−15.5	100
pSSCC—Rsoda	20.7	−62.5	−2.7	−14.1	100
sSSCC—ROccam	0.1	−62.4	−4.6	−33.0	100
sSSCC—RSoda	7.7	−72.4	−5.1	−14.8	100
9°S					
EUC—ROccam	0.0	−69.0	−20.0	−10.9	100
EUC—Rsoda	50.1	−36.6	−7.7	−5.6	100
pSSCC—ROccam	0.0	−68.3	−19.6	−12.1	100
pSSCC—Rsoda	24.2	−54.3	−9.0	−12.5	100
sSSCC—ROccam	28.8	−44.8	−17.6	−8.9	100
sSSCC—Rsoda	1.0	−62.3	−22.0	−14.8	100

[a]The relative contribution from physical (top) and biogeochemical (bottom) processes to the O_2 changes of the floats released into each equatorial source (EUC, pSSCC, and sSSCC) at the equatorial region (88°W) and arriving at the 9°S section expressed in % for both simulations: ROccam and RSoda. Percentages are calculated relatively to the sum of the absolute value of the tendency terms according to the Lagrangian experiment. The tendency of the processes to reduce or increase the O_2 concentration is indicated with a positive (source) or negative (sink) sign.

instance, the particles originating from the sSSCC exhibit large variations of the physical fluxes (see blue line in Figure 6c) at t ∼ 230 days (i.e., while reaching the coastal domain) that have no counterpart for the biogeochemical fluxes (see also the different scales in Figures 6a–6c). Thus, without discriminating the equatorial source, physical (mainly horizontal and vertical advection—not shown) and biogeochemical (mainly remineralization—not shown) fluxes present, relatively to their mean value, high regional and temporal variability expressed through occasional sharp fluctuations and changes in sign along the trajectories.

The much larger variability of the physical processes and biogeochemical processes is also observed over most of the OMZ (Figure 7). This results from the fact that, while rates of biologically induced O_2 changes are limited by substrates and biological process rates, physically induced O_2 changes are a product of transport rates and oxygen gradients, which induces large advection. Whereas it is expected that the physics dominate the O_2 fluxes offshore, in the coastal region, although biologically induced fluxes are increased due to the larger productivity and biomass availability, advection processes remain larger and highly variable due to the energetic coastal current system and mesoscale activity. Note that the magnitude of the variability shown in Figure 7 originates predominantly from intraseasonal variability (periods in the range of 3–120 days) rather than seasonal variability (not shown), which stresses the peculiar role played by mesoscale activity as a source of high-frequency variability for the OMZ dynamics.

We now focus on the differences in the simulated OMZ between RSoda and ROccam in terms of the magnitude and relative contribution of the individual processes. We have argued earlier that the difference in OMZ structure between ROccam and RSoda can be understood in terms of the different transport rates of deoxygenated waters by the sSSCC to the PCUC, which sets the background O_2 conditions. This difference in mean state implies a different balance between the advection tendency terms between ROccam and RSoda within the PCUC both at the entrance of the domain and across the PCUC (9°S) (Figure 8). Figure 8

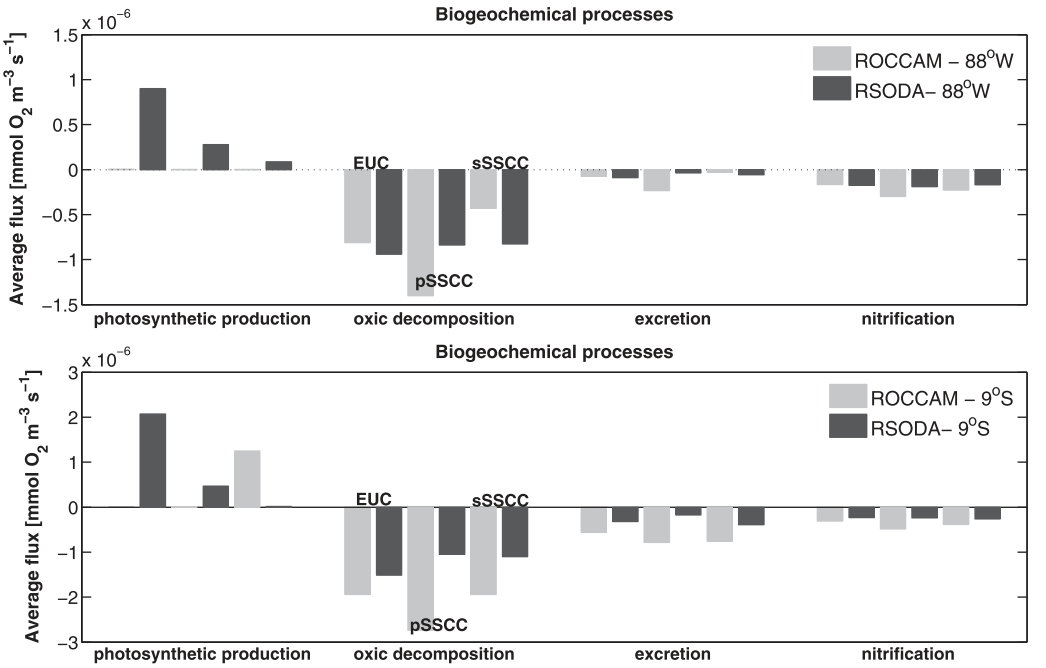

Figure 9. Mean flux of all O_2 terms involved in the biogeochemical processes of each equatorial subsurface current computed for both simulations, ROccam (black bars) and RSoda (gray bars), at (top) 88°W and (bottom) 9°S. Biogeochemical terms are referred to photosynthetic production (NO3P1, NO3P2, NO2P1, NO2P2, regP1, regP2), oxic decomposition (remoxD1, remoxD2, remoxDON), excretion (Z1met, Z2met), and nitrification (nitr1, nitr2). Fluxes with negative values represent a sink of oxygen and positive a source.

clearly indicates that, although the advection processes dominate in both simulations, their relative contributions to the total rate of O_2 changes are significantly different between the two simulations. At 88°W (Figure 8a), meridional advection in RSoda is a source term for all currents that is compensated by a loss due to horizontal advection, whereas the opposite is found for ROccam, i.e., zonal advection being a source and meridional advectional a sink. RSoda has also a much larger amplitude (by a factor of ∼20) of the advection terms compared to ROccam. At 9°S (Figure 8b), the zonal advection is a positive contribution to the rate of O_2 changes for the sSSCC in ROccam which is compensated by meridional advection, whereas meridional advection is a source term for the O_2 rate of changes compensated by both zonal and vertical advection in RSoda. The absolute oxygen fluxes of Figure 8 are converted into percentage contributions in Table 2, which emphasizes the differences between RSoda and ROccam in terms of the relative balance and role (source versus sink) between processes at 88°W and 9°S.

In terms of balance between biogeochemical fluxes (Figure 9), at 88°W, without discriminating the equatorial source, ROccam exhibits a higher oxygen consumption (mainly by oxic remineralization and nitrification) compared to RSoda. This feature is also found at 9°S (Figure 9b), except that the oxygen consumption is one order of magnitude larger in the coastal region due to high productivity being simulated there. Interestingly, the relative contribution of the different biogeochemical processes is comparable between both simulations, which are in contrast with the physical processes (see Table 2).

The larger sensitivity of the balance of physical processes to the open-boundary conditions compared to the biogeochemical processes can be understood as resulting from either the linear or nonlinear component of the advection process. The latter can be explained as follows: let us consider the differences between Rsoda and Roccam in terms of both circulation and local O_2 gradient, i.e.:

$$v_{Rsoda} = v_{ROccam} + \Delta v \text{ and } \left(\frac{\partial O_2}{\partial y}\right)_{Rsoda} = \left(\frac{\partial O_2}{\partial y}\right)_{Roccam} + \Delta O_2.$$

We consider here a change in meridional oxygen advection, but it applies similarly to zonal and vertical advection terms. Then, the difference in, say, mean meridional oxygen advection between Rsoda and Roccam can be written as follows:

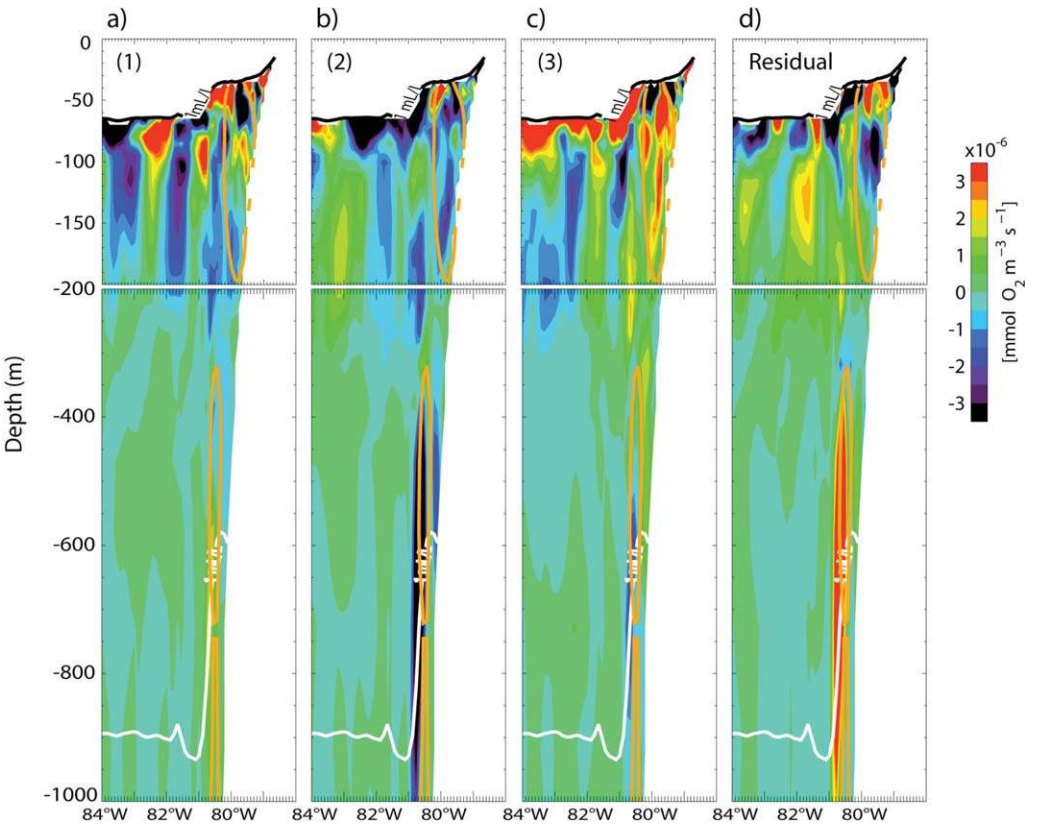

Figure 10. Contributions to the difference in mean meridional advection (Y18–Y20) between RSoda and ROccam at 9°S. The orange thick line indicates the −2 cm/s mean meridional current for RSoda. The thick black and white lines indicate the upper and lower OMZ limit for RSoda. The terms (a) (1), (b) (2), and (c) (3) are described in the text and the (d) residual represents an estimate of meridional diffusion.

$$(yadv)_{Rsoda} - (yadv)_{Roccam} = \overline{v_{soda} \cdot \left(\frac{\partial O_2}{\partial y}\right)_{Rsoda}} - \overline{v_{Roccam} \cdot \left(\frac{\partial O_2}{\partial y}\right)_{Roccam}}$$

that is:

$$\overline{v_{soda} \cdot \left(\frac{\partial O_2}{\partial y}\right)_{Rsoda}} - \overline{(v_{Rsoda} - \Delta v) \cdot \left(\left(\frac{\partial O_2}{\partial y}\right)_{Rsoda} - \Delta O_2\right)} = \overline{v_{Rsoda} \cdot \Delta O_2} + \overline{\Delta v \cdot \left(\frac{\partial O_2}{\partial y}\right)_{Rsoda}} - \overline{\Delta v \cdot \Delta O_2}. \quad (1)$$

The three terms on the right-hand side of equation (1) (referred to as terms (1), (2), and (3)) are the contributions to the difference in mean meridional advection between RSoda and ROccam, and allows interpreting the difference in total meridional advection evidenced from Figure 8.

Figure 10 presents the results for a section at 9°S, which indicates that the different terms of the difference in meridional advection between RSoda and ROccam have a comparable magnitude. This means that the difference between the two simulations cannot be attributed in a straightforward manner to differences in mean circulation. Rather, it is the combined effect of both the difference in mean circulation and the difference in O_2 spatial distribution that explains the large difference in the balance of the O_2 budget (cf. Figure 8). Note that term 3 ($\overline{\Delta v . \Delta O_2}$) corresponds to the nonlinear contribution to the difference in advection between the two simulations. Since its contribution is as large as terms (1) and (2), we may speculate that the OMZ dynamics in this region is likely nonlinear, which is consistent with the fact that our model configuration is sensitive to slight differences in boundary conditions. The estimate of the contribution of meridional diffusion (residual) also suggests that this term is a key contributor to the O_2 changes in the lower part of the OMZ near the coast.

4. Conclusions

In this study, a high-resolution coupled physical/biogeochemical model is used to investigate the dynamics of the OMZ off Peru. The focus is on the sensitivity of the OMZ's oxygen budget to the ocean boundary conditions in the tropical region, taking advantage of a previous study that analyzed in details the circulation of the same model configuration [*Montes et al*., 2010]. Our analysis suggests that there is a large sensitivity of the OMZ to the mean tropical circulation characteristics. Although the differences in the mean circulation of the OBCs are small between the model configurations [*Montes et al*., 2010; *Echevin et al*., 2011], the resulting simulated OMZs exhibit significant differences both in terms of O_2 concentration patterns within and near the OMZ. From a Lagrangian perspective, such differences are shown to result to a large extent from differences in the magnitude of the transport of oxygenated waters from the sSSCC that lead to a different balance between biogeochemical and physical processes within the oxycline. In particular, in the simulation where the transport of deoxygenated and nutrient-rich waters from the sSSCC is larger, remineralization attributed to biological export production is larger and yields anoxic conditions and a more intense OMZ. We further show that the contrasted balance between physical processes between the two simulations, in particular for advection, results from changes in both currents and O_2 gradients and not predominantly from changes in currents alone. Therefore, despite the much smaller (by one order of magnitude) variability in biogeochemically induced oxygen fluxes compared to physical fluxes, the former are essential for the OMZ dynamics.

Our interpretation is complicated by the fact that both configurations lead to different levels of eddy kinetic energy (EKE) due to slight differences in the mean vertical structure of the coastal current. In particular, the difference in mesoscale activity resulting from differences in the intensity of the upwelling fronts [*Marchesiello et al*., 2003] may contribute to eroding or expanding the upper bound of the OMZ more in one model configuration as compared to the other. Recently, *Gruber et al*. [2011] showed that mesoscale activity tended to reduce the biological production and export in coastal upwelling regions as also seen in other high-resolution models [e.g., *Oschlies*, 2002], which can be influential on the OMZ. The approach designed in *Gruber et al*. [2011] could be easily applied to our coupled model (i.e., switching off the nonlinear terms in the momentum equations) to study the sensitivity of the OMZ to mesoscale activity. However, such an approach will also lead to modifications of the characteristics of the main pathways described in the paper due to the nonlinear interaction between mean currents and mesoscale activity, which would make the analysis more complicated. At this stage, it is interesting to note that the simulation exhibiting the largest EKE, i.e., RSoda, is associated with a smaller OMZ than the one simulated in ROccam which also has lower EKE level. The detailed investigation of the role of mesoscale activity on the OMZ requires additional model experiment, which is beyond the scope of the present paper.

The results of our sensitivity experiment may have implications for the interpretation of results of global coupled models. Considering the important role of the sSSCC on the OMZ identified in our study, we may wonder if failure of current-generation global models in realistically simulating the OMZ [*Cocco et al*., 2013] may originate from difficulties in representing the details of the Equatorial Current System in the eastern Pacific. The large spread of IPCC class models in simulating the Eastern South Pacific OMZ is consistent with this remark [*Stramma et al*., 2012]. This calls for further studies using a high-resolution coupled biogeochemical model for documenting the OMZ dynamics in the Eastern Pacific. We show here that the oxygen flux into the PCUC is determined by both the circulation and the oxygen concentrations at the westward boundary, which puts a further constraint on the open-boundary conditions. Under climatological forcing, our model leads to a realistic OMZ that, according to the Lagrangian diagnostics, is mostly constrained by the inflow conditions and regional physics rather than regional biogeochemistry. However, its characteristics near the coast also depend on the balance between physical and biogeochemical processes because mixing is enhanced and the upwelling is strongest. It is currently unclear to what extent this climatological steady state balance also holds on interannual time scales considering that the equatorial circulation can experience drastic changes at low frequency (i.e., ENSO) that substantially affect the coastal upwelling system. Work presently under way with the same model is devoted to such an investigation of interannual variability.

Appendix A: Biogeochemical Model for the Eastern Boundary Upwelling Systems (BioEBUS)

BioEBUS is a nitrogen-based model, originally developed to simulate the first trophic levels of the Benguela ecosystem [*Gutknecht et al*., 2013a, 2013b], deriving from the $N_2P_2Z_2D_2$ version of *Koné et al*. [2005]. In the

Table A1. Parameter Values for the ETP Biogeochemical Model[a]

Parameter	Symbol	Units	Values
Phytoplankton			
Maximum growth rate for P_L	$a\ P_L$	d^{-1}	0.4
Detritus			
Hydrolysis rate of D_s	$m\ D_s$	d^{-1}	0.06
Hydrolysis rate of D_L	$m\ D_L$	d^{-1}	0.04
Mineralization in Oxic Conditions			
Half saturation constant	K_{OX}	mmol O_2 m^{-3}	55
Nitrification			
Rate of first stage of nitrification	K_{N32}	d^{-1}	0.09
Rate of second stage of nitrification	K_{N24}	d^{-1}	0.25
Anammox			
Anammox constant	$K_{Anammox}$	d^{-1}	0.1

[a]The remaining references are kept as in the original version of Benguela (see *Gutknecht et al.* [2013a, 2013b]).

model, an advection-diffusive equation determines the evolution of any biological tracer concentration. Bio-EBUS contains 12 compartments. Phytoplankton, zooplankton, and detritus compartments are split each one into two state variables based on a size criterion: phytoplankton (small—flagellates P_s, large—diatoms P_L), zooplankton (small—ciliates Z_s, large—copepods Z_L), and detritus (small (D_s) and large (D_L) particles). The model includes a dissolved organic nitrogen (DON) [*Kirchman et al*., 1993; *Carslon and Ducklow*, 1995] compartment, three dissolved inorganic nutrients (NO_3, NO_2, and NH_4) to have a more detailed description of a microbial loop [ammonification/nitrification processes under oxic conditions and, nitrification/denitrification/anammox under suboxic conditions, *Yakusev et al*., 2007], an oxygen equation to support the oxygen-dependent processes [*Peña et al*., 2010] and, a parameterization to determinate the N_2O production [*Suntharalingam et al*., 2000, 2012].

In order to get a more realistic solution for the ETP model, the model parameters were tuned to simultaneously fit modeled oxygen and nitrate fields to observations (see Table A1 for derived values). These changes as compared to the Benguela version were motivated by the need to adjust the microbiological rates to values observed in the ETP which are different from those in the Benguela system.

Acknowledgments
We thank the EUR-OCEANS Consortium for providing the postdoctoral funding for I.M. (Flagship EUR-OCEANS referenced as EOC/PFB/PC/2011.0013) as well as the Deutsche Forschungsgemeinschaft via the Sonderforschungsbereich 754 "Climate-Biogeochemistry Interactions in the Tropical Ocean" for supporting this study. We also thank E. Des Barton and three anonymous reviewers for their comments and suggestions that helped improving the manuscript. This work used HPC resources from CALMIP (grant 2011-[P1134]) and of the cluster of PCs of the CIMOBP/IRD (SPIRALES/DSI/IRD). The CNES and ESA are also acknowledged for their support (project OST-ST SOUTH-EBUS, and STSE Oceanflux-Upwelling Theme grant 400014715/11/I-NB, respectively).

References

Albert, A., V. Echevin, M. Lévy, and O. Aumont (2010), Impact of nearshore wind stress curl on coastal circulation and primary productivity in the Peru upwelling system, *J. Geophys. Res.*, *115*, C12033, doi:10.1029/2010JC006569.

Atkinson, L. P., J. Huthnance, and J. Blanco (2004), Circulation, mixing and the distribution of remineralized nutrients, in *The Sea*, vol. 13, edited by A. R. Robinson, J. McCarthy, and B. J. Rothschild, pp. 227–267, Harvard Univ. Press.

Bianchi, D., J. P. Dunne, J. L. Sarmiento, and E. D. Galbraith (2012), Data-based estimates of suboxia, denitrification, and N_2O production in the ocean and their sensitivities to dissolved O_2, *Global Biogeochem. Cycles*, *26*, GB2009, doi:10.1029/2011GB004209.

Brandt, P., V. Hormann, A. Kortzinger, M. Visbeck, G. Krahmann, L. Stramma, R. Lumpkin, and C. Schmid (2010), Changes in the ventilation of the oxygen minimum zone of the Tropical North Atlantic, *J. Phys. Oceanogr.*, *40*, 1784–1801.

Capet, X. J., P. Marchesiello, and J. C. McWilliams (2004), Upwelling response to coastal wind profiles, *Geophys. Res. Lett.*, *31*, L13311, doi:10.1029/2004GL020123.

Carr, S., X. Capet, J. McWilliams, J. T. Pennington, and F. P. Chavez (2008), The influence of diel vertical migration on zooplankton transport and recruitment in an upwelling region: Estimates from a coupled behavioral-physical model, *Fish. Oceanogr.*, *17*, 1–15.

CARS (2009), CSIRO Marine and Atmospheric Research CSIRO Atlas of Regional Seas. [Available at http://www.marine.csiro.au/~dunn/cars2009/.]

Carslon, C. A., and H. W. Ducklow (1995), Dissolved organic carbon in the upper ocean of the central equatorial Pacific Ocean, 1992: Daily and finescale vertical variations, *Deep Sea Res., Part II*, *42*, 639–656, doi:10.1016/0967-0645(95)00023-J.

Carton, J. A., and B. S. Giese (2008), A reanalysis of ocean climate using Simple Ocean Data Assimilation (SODA), *Mon. Weather Rev.*, *136*, 2999–3017.

Chavez, F. P., A. Bertrand, R. Guevara-Carrasco, P. Soler, and J. Csirke (2008), The northern Humboldt Current System: Brief history, present status and a view towards the future, *Prog. Oceanogr.*, *79*, pp. 95–105.

Clarke, A. J., and R. Ahmed (1999), Dynamics of remotely forced intraseasonal oscillations off the Western Coast of South America, *J. Phys. Oceanogr.*, *29*, 240–258.

Cocco, V., et al. (2013), Oxygen and indicators of stress for marine life in multi-model global warming projections, *Biogeosciences*, *10*, 1849–1868, doi:10.5194/bg-10–1849-2013.

Colas, F., X. Capet, J. C. McWilliams, and A. F. Shchepetkin (2008), 1997–1998 El Niño off Peru: A numerical study, *Prog. Oceanogr.*, *79*, 138–155.

Czeschel, R., L. Stramma, F. U. Schwarzkopf, B. S. Giese, A. Funk, and J. Karstensen (2011), Middepth circulation of the eastern tropical South Pacific and its link to the oxygen minimum zone, *J. Geophys. Res.*, *116*, C01015, doi:10.1029/2010JC006565.

Da Silva, A. M., C. C. Young, and S. Levitus (1994), Atlas of surface marine data 1994, vol. 1, Algorithms and procedures, *Tech. Rep. 6*, U.S. Department of Commerce, NOAA, NESDIS, Natl. Oceanogr. and Atmos. Admin., Silver Spring, Md.

Dewitte, B., S. Illig, L. Renault, K. Goubanova, K. Takahashi, D. Gushchina, K. Mosquera, and S. Purca (2011), Modes of covariability between sea surface temperature and wind stress intraseasonal anomalies along the coast of Peru from satellite observations (2000–2008), *J. Geophys. Res.*, *116*, C04028, doi:10.1029/2010JC006495.

Dewitte, B., et al. (2012), Change in El Niño flavours over 1958–2008: Implications for the long-term trend of the upwelling off Peru, *Deep Sea Res., Part II*, *77–80*, 143–156, doi:10.1016/j.dsr2.2012.04.011.

Echevin, V., F. Colas, A. Chaigneau, and P. Penven (2011), Sensitivity of the Northern Humboldt Current System nearshore modeled circulation to initial and boundary conditions, *J. Geophys. Res.*, *116*, C07002, doi:10.1029/2010JC006684.

Enfield, D. B. (1987), The intraseasonal oscillation in Eastern Pacific sea levels: How is it forced?, *J. Phys. Oceanogr.*, *17*, 1860–1876.

Fuenzalida, R., W. Schneider, J. Garces, L. Bravo, and C. Lange (2009), Vertical and horizontal extension of the oxygen minimum zone in the eastern South Pacific Ocean, *Deep Sea Res., Part II*, *56*, 992–1003, doi:10.1016/j.dsr2.2008.11.001.

Furue, R., J. P. McCreary, Z. Yu, and D. Wang (2007), The dynamics of the southern Tsuchiya Jet, *J. Phys. Oceanogr.*, *37*, 531–553, doi:10.1175/JPO3024.1.

Gnanadesikan, A., J. P. Dunne, and J. John (2012), Understanding why the volume of suboxic waters does not increase over centuries of global warming in an Earth System Model, *Biogeosciences*, *9*, 1159–1172, doi:10.5194/bg-9–1159-2012.

Gruber, N., Z. Lachkar, H. Frenzel, P. Marchesiello, M. Münnich, J. C. McWilliams, T. Nagai, and G. K. Plattner (2011), Eddy-induced reduction of biological production in eastern boundary upwelling systems, *Nat. Geosci.*, *4*, 787–792, doi:10.1038/NGEO01273.

Gutknecht, E., et al. (2013a), Coupled physical/biogeochemical modeling including O_2-dependent processes in Eastern Boundary Upwelling Systems: Application in the Benguela, *Biogeosciences*, *10*, 3559–3591, doi:10.5194/bg-10-1-2013.

Gutknecht, E., et al. (2013b), Nitrogen transfers off Walvis Bay: A 3-D coupled physical/biogeochemical modeling approach in the Namibian Upwelling System, *Biogeosciences*, *10*, 4117–4135, doi:10.5194/bg-10–4117-2013.

Hamersley, M. R., L. Gaute, D. Woebken, J. E. Rattray, E. C. Hopmans, and J. S. Sinninghe (2007), Anaerobic ammonium oxidation in the Peruvian oxygen minimum zone, *Limnol. Oceanogr.*, *52*, 923–933.

Helly, J. J., and L. A. Levin (2004), Global distribution of naturally occurring marine hypoxia on continental margins, *Deep Sea Res., Part I*, *51*, 1159–1168.

Huyer, A., R. L. Smith, and T. Paluszkiewicz (1987), Coastal upwelling off Peru during normal and El Niño times, *J. Geophys. Res.*, *92*, 14,297–14,307, doi:10.1029/JC092iC13p14297.

Ishida, A., H. Mitsudera, Y. Kashino, and T. Kadokura (2005), Equatorial Pacific subsurface countercurrents in a high-resolution global ocean circulation model, *J. Geophys. Res.*, *110*, C07014, doi:10.1029/2003JC002210.

Kalvelage, T., M. M. Jensen, N. P. Revsbech, P. Lam, G. Lavik, and M. M. M. Kuypers (2012) Oxygen sensitivity of Anammox and coupled n-cycle processes in oxygen minimum zones, *PLoS One*, *6*(12), e29299, doi:10.137/journal.pone.0029299.

Kamykowsi, D. Z., and S. J. Zentara (1990), Hypoxia in the world ocean as recorded in the historical data set, *Deep Sea Res., Part A*, *37*, 1861–1874.

Karstensen, J., L. Stramma, and M. Visbeck (2008), Oxygen minimum zones in the eastern tropical Atlantic and Pacific oceans, *Prog. Oceanogr.*, *77*, 331–350.

Keeling, R. F., and H. E. Garcia (2002), The change in oceanic O2 inventory associated with recent global warming, *Proc. Natl. Acad. Sci. U. S. A.*, *99*, 7848–7853.

Kessler, W. S. (2006), The circulation of the eastern tropical Pacific: A review, *Prog. Oceanogr.*, *69*, 181–217.

Kirchman, D. L., C. Lancelot, M. Fasham, L. Legendre, G. Radach, and M. Scott (1993), Dissolved organic matter in biogeochemical models in the ocean, in *Towards a Model of Ocean Biogeochemical Processes*, NATO ASI Series, vol. 10, pp. 209–225, Springer-Verlag, Berlin Heidelberg.

Koné, V., E. Machu, P. Penven, V. Garçon, P. Freon, and H. Demarcq (2005), Modeling the primary and secondary productions of the southern Benguela upwelling system: A comparative study through two biogeochemical models, *Global Biogeochem. Cycles*, *19*, GB4021, doi:10.1029/2004GB002427.

Lam, P., G. Lavik, M. Jensen, J. V. de Vossenberg, M. Schmid, D. Woebken, D. Gutiérrez, R. Amann, M. S. M. Jetten, and M. Kuypers (2009), Revising the nitrogen cycle in the Peruvian oxygen minimum zone, *Proc. Natl. Acad. Sci. U. S. A.*, *106*(12), 4752–4757, doi:10.1073/pnas.0812444106.

Liu, W. T., W. Tang, and P. S. Polito (1998), NASA scatterometer provides global ocean-surface wind fields with more structures than numerical weather prediction, *Geophys. Res. Lett.*, *25*, 761–764.

Lukas, R. (1986), The termination of the equatorial undercurrent in the Eastern Pacific, *Prog. Oceanogr.*, *16*, 63–90.

Marchesiello, P., J. C. McWilliams, and A. Shchepetkin (2003), Equilibrium structure and dynamics of the California Current System, *J. Phys. Oceanogr.*, *33*, 753–783.

McClain, C. R., M. L. Cleave, G. C. Feldman, W. W. Gregg, S. B. Hooker, and N. Kuring (1998), Science quality SeaWiFS data for global biosphere research, *Sea Technol.*, *39*(9), 10–16.

Monteiro, P., A. Van der Plas, V. Mohrholz, E. Mabille, A. Pascall, and W. Joubert (2006), Variability of natural hypoxia and methane in a coastal upwelling system: Oceanic physics or shelf biology?, *Geophys. Res. Lett.*, *33*, L16614, doi:10.1029/2006GL026234.

Monteiro, P. M. S., B. Dewitte, M. I. Scranton, A. Paulmier, and A. van der Plas (2011), The role of open ocean boundary forcing on seasonal to decadal-scale variability and long-term change of natural shelf hypoxia, *Environ. Res. Lett.*, *6*, 025002, doi:10.1088/1748–9326/6/2/025002.

Montes, I., F. Colas, X. Capet, and W. Schneider (2010), On the pathways of the equatorial subsurface currents in the Eastern Equatorial Pacific and their contributions to the Peru-Chile Undercurrent, *J. Geophys. Res.*, *115*, C09003, doi:10.1029/2009JC005710.

Morales, C. E., S. E. Hormazabal, J. L. Blanco (1999), Interannual variability in the mesoscale distribution of the depth of the upper boundary of the oxygen minimum layer off northern Chile (18–24S): Implications for the pelagic system and biogeochemical cycling, *J. Mar. Res.*, *57*, pp. 909–932.

Morel, A., and J. F. Berthon (1989), Surface pigments, algal biomass profiles, and potential production of euphotic layer: Relationship reinvestigated in view of remote-sensing applications, *Limnol. Oceanogr.*, *34*, 1545–1562.

O'Reilly, J. E., et al. (2000), Ocean chlorophyll a algorithms for SeaWiFS, OC2, and OC4: Version 4, in *SeaWiFS Postlaunch Calibration and Validation Analyses, Part 3, NASA Tech. Memo 2000–206892*, vol. 11, edited by J. E. O'Reilly et al., pp. 9–19, NASA, Goddard Space Flight Center, Greenbelt, Maryland.

Oschlies, A. (2002), Can eddies make ocean deserts bloom?, *Global Biogeochem. Cycles*, *16*(4), 1106, doi:10.1029/2001GB001830.

Paulmier, A., and D. Ruiz-Pino (2009), Oxygen minimum zones (OMZs) in the modern ocean, *Prog. Oceanogr.*, *80*(3–4), 113–128, doi:10.1029/j.pocean.2008.08.001.

Paulmier, A., D. Ruiz-Pino, V. Garcon, and L. Farias (2006), Maintaining of the East South Pacific Oxygen Minimum Zone (OMZ) off Chile, *Geophys. Res. Lett.*, *33*, L20601, doi:10.1029/2006GL026801.

Peña, M. A., S. Katsev, T. Oguz, and D. Gilbert (2010), Modeling dissolved oxygen dynamics and hypoxia, *Biogeosciences*, *7*, 933–957.
Penven, P., V. Echevin, J. Pasapera, F. Colas, and J. Tam (2005), Average circulation, seasonal cycle, and mesoscale dynamics of the Peru Current System: A modeling approach, *J. Geophys. Res.*, *110*, C10021, doi:10.1029/2005JC002945.
Ramos, M., B. Dewitte, O. Pizarro, and G. Garric (2008), Vertical propagation of the extra-tropical Rossby wave during the 1997/98 El Niño off the west coast of South-America in a medium-resolution OGCM simulation, *J. Geophys. Res.*, *113*, C08041, doi:10.1029/2007JC004681.
Saunders, P. M., A. C. Coward, and B. A. De Cuevas (1999), Circulation of the Pacific Ocean seen in a global ocean model (OCCAM), *J. Geophys. Res.*, *104*, 18,281–18,299, doi:10.1029/1999JC900091.
Shchepetkin, A. F., and J. C. McWilliams (2005), The regional oceanic modeling system (ROMS): A split-explicit, free-surface, topography-following-coordinate oceanic model, *Ocean Modell.*, *9*, 347–404.
Shchepetkin, A. F., and J. C. McWilliams (2009), Correction and commentary for "Ocean forecasting in terrain-following coordinates: Formulation and skill assessment of the regional ocean modeling system" by Haidvogel et al., *J. Comp. Phys.*, *227*, 3595–3624.
Smith, W. H. F., and D. T. Sandwell (1997), Global seafloor topography from satellite altimetry and ship depth soundings, *Science*, *277*, 1957–1962.
Stramma, L., G. C. Johnson, E. Firing, and S. Schmidtko (2010), Eastern Pacific oxygen minimum zones: Supply paths and multidecadal changes, *J. Geophys. Res.*, *115*, C09011, doi:10.1029/2009JC005976.
Stramma, L., A. Oschlies, and S. Schmidtko (2012), Mistmatch between observed and modeled trends in dissolved upper-ocean oxygen over the last 50 yr, *Biogeosciences*, *9*(10), 4045–4057, doi:10.5194/bg-9–4045-2012.
Suntharalingam, P., J. L. Sarmiento, and J. R. Toggweiler (2000), Global significance of nitrous-oxide production and transport from oceanic low-oxygen zones: A modeling study, *Global Biogeochem. Cycles*, *14*, 1353–1370.
Suntharalingam, P., E. Buitenhuis, C. Le Quere, F. Dentener, C. Nevinson, L. Butler, H. Bange, and G. Forster (2012), Quantifying the impact of anthropogenic nitrogen deposition on oceanic nitrous oxide, *Geophys. Res. Lett.*, *39*, L07605, doi:10.1029/2011GL050778.
Taylor, K. E. (2001), Summarizing multiple aspects of model performance in a single diagram, *J. Geophys. Res.*, *106*, 7183–7192, doi:10.1029/2000JD900719.
Vega, A., Y. du-Penhoat, B. Dewitte, and O. Pizarro (2003), Equatorial forcing of internannual Rossby waves in the Eastern South Pacific, *Geophys. Res. Lett.*, *30*(5), 1197, doi:10.1029/2002GL015886.
Wyrtki, K. (1962), The oxygen minima in relation to ocean circulation, *Deep Sea Res. Oceanogr. Abstr.*, *9*, 11–23.
Yakusev, E. V., F. Pollehne, G. Jost, I. Kuznetso, B. Schneider, and L. Urnlauf (2007), Analysis of the water column oxic/anoxic interface in the Black and Baltic seas with a numerical model, *Mar. Chem.*, *107*, 388–410, doi:10.1016/j.marchem.2007.06.003.